NeuroImage 199 (2019) 228–236

Contents lists available at ScienceDirect

NeuroImage

journal homepage: www.elsevier.com/locate/neuroimage

Selective spatial attention involves two alpha-band components associated with distinct spatiotemporal and functional characteristics

Jianrong Jia [a,b,c,d], Fang Fang [a,b,c,d,**], Huan Luo [a,b,c,*]

[a] School of Psychological and Cognitive Sciences and Beijing Key Laboratory of Behavior and Mental Health, Peking University, Beijing, China
[b] IDG/McGovern Institute for Brain Research, Peking University, Beijing, China
[c] Key Laboratory of Machine Perception (Ministry of Education), Peking University, Beijing, China
[d] Peking-Tsinghua Center for Life Sciences, Peking University, Beijing, China

ARTICLE INFO

Keywords:
Selective attention
Spatial attention
EEG
TRF
Alpha-band

ABSTRACT

Attention is crucial for efficiently coordinating resources over multiple objects in a visual scene. Recently, a growing number of studies suggest that attention is implemented through a temporal organization process during which resources are dynamically allocated over a multitude of objects, yet the associated neural evidence, particularly in low-level sensory areas, is still limited. Here we used EEG recordings in combination with a temporal response function (TRF) approach to examine the spatiotemporal characteristics of neuronal impulse response in covert selective attention. We demonstrate two distinct alpha-band components – one in post-central parietal area and one in contralateral occipital area – that are involved in coordinating neural representations of attended and unattended stimuli. Specifically, consistent with previous findings, the central alpha-band component showed enhanced activities for unattended versus attended stimuli within the first 200 ms temporal lag of TRF response, suggesting its inhibitory function in attention. In contrast, the contralateral occipital component displayed relatively earlier activation for the attended than unattended one in the TRF response. Furthermore, the central component but not the occipital component was correlated with attentional behavioral performance. Finally, the parietal area exerted directional influences on the occipital activity through alpha-band rhythm. Taken together, spatial attention involves two hierarchically organized alpha-band components that are associated with distinct spatiotemporal characteristics and presumably play different functions.

1. Introduction

Attention is a core cognitive function important for coordinating the limited resources among multiple locations, features, and objects in a visual scene to deal with various tasks and environments (Carrasco, 2011). It is widely known that selective attention would facilitate behavioral performance and enhance the corresponding neural responses so that the attended location wins the competition over the others (Desimone, 1998; Desimone and Duncan, 1995; Tsotsos, 1990). Interestingly, a growing number of recent studies, by taking a temporal perspective, suggest that attention might not be as sustained as previously posited, but involves a temporal organization process during which attentional resources are dynamically allocated among a multitude of objects (Buschman and Kastner, 2015; Fries, 2015; Large and Jones, 1999; Schroeder and Lakatos, 2009). Notably, a series of recent behavioral studies, by using a time-resolved psychophysical measurement, have shown that attention samples locations, objects, perceptual predictions, and information channels in a rhythmic switching manner (Davidson et al., 2018; Fiebelkorn et al., 2013; Ho et al., 2017; Huang et al., 2015; Landau and Fries, 2012; Song et al., 2014; Wang and Luo, 2017).

On the other hand, the associated neural evidence is still very limited (Fiebelkorn et al., 2018; Helfrich et al., 2018; Landau et al., 2015). Recently, by using a temporal response function (TRF) method to tag and dissociate object-specific neuronal responses in multi-object attentional task, Jia et al. (2017) showed that even when attention is instructed to

* Corresponding author. School of Psychological and Cognitive Sciences, Peking University, PKU-IDG/McGovern Institute for Brain Science, Peking University, 52 Haidian Road, Beijing, 100087, China.
** Corresponding author. School of Psychological and Cognitive Sciences, Peking University, PKU-IDG/McGovern Institute for Brain Science, Peking University, Peking-Tsinghua Center for Life Sciences, Peking University, 52 Haidian Road, Beijing, 100087, China.
E-mail addresses: ffang@pku.edu.cn (F. Fang), huan.luo@pku.edu.cn (H. Luo).

https://doi.org/10.1016/j.neuroimage.2019.05.079
Received 30 August 2018; Received in revised form 12 May 2019; Accepted 29 May 2019
Available online 30 May 2019

completely or largely dwell on one object, the TRF response displayed a shift from the attended one to unattended one through dynamic modulation of inhibitory alpha-band activations. Specifically, there is an "inhibition followed by rebound" alpha-band pattern when comparing the attended and unattended TRF responses, suggesting that attention first samples the attended object via inhibiting the unattended one, and then switches to the unattended object by instead inhibiting the attended one, in terms of the relative timing in the neural impulse response.

However, several critical issues remain unknown. First, the reported temporal profiles for attentional processing was based on the direct comparisons between the attended and unattended conditions, and thus could not determine the exact underlying processes. For example, the initial alpha-band decrease for unattended (Unatt) versus attended (Att) condition might be caused by the reduced Att alpha-band response (inhibition release) or increased Unatt alpha-band activation (suppression enhancement), or both. Second, previous results only demonstrated the engagement of a presumably high-level area (i.e., central parietal electrodes) in this process, and how the dynamic profiles modulate the neuronal activations in the low-level sensory areas still remains unknown.

The current study aims to address the two unclear issues as stated above. First, a neutral condition was added to be compared with the attended and unattended conditions respectively so that the two possible underlying processes could be dissociated and assessed separately. Second, we further examined how this dynamic attentional processing modulates the sensory processing in low-level areas. Our results demonstrate two alpha-band components in TRF responses – one in postcentral parietal area and one in contralateral occipital area – that are involved in selective spatial attention. The central alpha-band components replicated our previous findings (Jia et al., 2017) and showed enhanced alpha-band response for the unattended location compared to attended one within the first 200 ms temporal lag. In contrast, the occipital component was location-dependent (i.e., contralateral) and showed an attended-followed-by-unattended response profile in the TRF response. The central alpha-band component but not the occipital component was correlated with attentional behavioral performance. Finally, the parietal area exerted directional influences on the occipital activity through alpha-band rhythm. Taken together, we propose that spatial attention involves two hierarchically organized alpha-band components, which are associated with distinct characteristics and presumably play different functions in coordinating attentional resources over multiple locations.

2. Materials and methods

2.1. Participants

Twenty participants aged 17–24 were recruited (Main experiment: N = 14; Control experiment: N = 6), and no one had participated in our previous study (Jia et al., 2017). All participants had normal or corrected-to-normal vision and had no history of psychiatric or neurological disorders. All experiments were carried out in accordance with the Declaration of Helsinki. All participants were provided written informed consent prior to the start of the experiment, which was approved by the Research Ethics Committee at Peking University.

2.2. Stimuli and tasks

Participants sat in a dark room in front of a CRT monitor (100 Hz refresh rate) with their head stabilized on a chin rest. In the practice session, subjects were trained on the task and to maintain central fixation as well as minimizing eye blinks throughout each trial. In each trial of the main experiment, they fixated on a central fixation spot and then two discs were displayed simultaneously in the left and right visual fields for 5 s. Participants were requested to maintain central fixation throughout each trial and to covertly monitor the possible appearance of a target square (side length of 3.75°) within 1 of the 2 peripheral discs (radius of 5.5°) that were presented at 7.5° to either side of the fixation point (Fig. 1). The target square was presented for 0.5 s and occurred at a random time between 0.25 s and 4.25 s of the 5 s trial in 25% of the trials. At the end of each trial, participants pressed 1 of 2 buttons to report whether they had detected the target. All trials were included into the data analysis to increase the signal to noise ratio. Across trials, the contrast of the target square (i.e., target luminance relative to the momentary background disc luminance) was adjusted according to the detection accuracy (using a 3-down-1-up staircase procedure), so that the overall target detection performance was maintained at around 80%.

Participants' spatial attention was manipulated by a central cue. The main experiment employed a block design that consisted of two blocks of cueing trials and two blocks of neutral trials. Each block contained sixty trials. The cueing blocks used the same experimental paradigm as that in previous study (Jia et al., 2017). Specifically, at the beginning of each trial of cueing block, a central arrow cue (1-s duration) was presented to indicate which side (left or right) the participants should attend to for target detection (Fig. 1A). The target only appeared in the cued disc (100% cue validity), and participants were informed of the cue validity in advance. In each trial of the neutral blocks (Fig. 1B), the central diamond cue did not contain any target location information (bidirectional) and the target would appear at either the left or right visual field with equal probability. Subjects therefore needed to attend to both of the two discs. Participants were also informed of the cue validity before the experiment and noticed that they should monitor the 2 discs simultaneously. The order of the blocks was balanced within and between participants. The control experiment was the same as the main experiment except that the cueing and neutral conditions were randomly mixed within blocks. The control experiment had 3 blocks of 60 trials, with 120 cueing trials and 60 neutral trials.

All participants in both experiments were trained to maintain central fixation before the experiment and were instructed to keep the number of eye blinks to a minimum during the experimental trials. Eye movements in control experiment were monitored using an EyeLink 1000 eye-tracker (SR Research), and fixation was required within a 1° visual angle of the fixation point to initiate the experimental trials. The results showed that the participants maintained good fixation at the central cross (within 1°).

2.3. Luminance modulation

During each trial, the luminance of the 2 discs was independently modulated at each frame refresh (100 Hz monitor refresh rate) between black (0 cd/m^2) to white (84.6 cd/m^2) according to 2 random 5 s temporal sequences that were generated anew in each trial. The CRT refresh rate of 100 Hz allowed us to present temporal frequencies ranging between 0 and 50 Hz. Each random sequence was first whitened to have equal power at all frequencies. Specifically, each sequence was transformed to frequency domain through Fourier transform and then normalized in amplitudes before transforming back to time series using inverse Fourier transform.

2.4. EEG acquisition and preprocessing

EEG signals were recorded continuously using 2 BrainAmp amplifiers and a 64-channel ActiCap (BrainProducts), and were first preprocessed using the FieldTrip toolbox (Oostenveld et al., 2011). Horizontal and vertical electrooculograms were recorded by 2 additional electrodes around the participants' eyes. EEG data were re-referenced to the average value of all channels and were offline band-pass filtered between 2 and 50 Hz using a Butterworth IIR filter with the order of 2. Independent component analysis was then performed to remove eye-movement and artifact components, and the remaining components were back-projected onto the EEG electrode space. The EEG was then downsampled to 100 Hz as the same sampling frequency of the luminance sequences for further TRF calculation. The 0.5–4.5 s of the luminance sequence and its

corresponding EEG signal were then entered in the TRF estimation to avoid the influence of the onset and offset response, resulting in the TRF response as a function of temporal lag (0–0.8 s).

2.5. Data analysis

2.5.1. TRF computation

The temporal responses function (TRF) was calculated using the multivariate temporal response function (mTRF) toolbox (Crosse et al., 2016; Lalor et al., 2006). By considering the brain in simplified form as a linear system, the TRF describes the linear part of the brain's transformation of a stimulus input, S(t), to the neural response output, R(t), as R(t) = TRF * S(t), where * denotes the convolution operator. Specifically, the TRF computation was performed by a regularized linear regression (Fig. 1C), with the lambda parameter set to 1 to control overfitting. Notably, the TRF response represents the neural impulse response, with the time axis indicating the latency after each unit transient of the stimulus sequence, thus characterizing a relative-time signal instead of absolute-time EEG course. The stimulus luminance sequences and EEG signals were concatenated across trials respectively and then transformed to z score before TRF calculation. This was done for each condition, each sensor and in each subject separately. The 4 s signal of each trial and at least 120 trials for each condition provided enough signal duration for TRF response estimation (Lalor et al., 2006).

The TRF method, to some extent, is a generalization of the conventional visual evoked response (VEP) technique (Crosse et al., 2016; Lalor et al., 2006). Meanwhile, different from the typical VEP approach, the TRF method allows response estimation for a unit transient from a continuously-changing stimulus, and thus could achieve an ecological investigation of the properties of the visual system. Moreover, TRF is advantageous over VEP in that it could tag multiple items by applying independent luminance sequences in single trials, thus enabling the dissociation of the neural response for each item from the same EEG recordings.

2.5.2. Time-frequency analysis

The obtained TRF responses were then analyzed with MATLAB (MathWorks, Inc., Natick, Massachusetts), using the wavelet toolbox functions to examine their spectrotemporal power profiles as a function of frequency and time. The TRF temporal profile was transformed using the continuous complex Gaussian wavelet transform, with frequencies ranging from 1 to 30 Hz in increments of 1 Hz. This time-frequency analysis was performed for each condition, for each stimulus (left and right), on each channel, and in each participant separately.

2.5.3. Correlation between behavioral and neural attentional effects

Indices for behavioral and neural attentional effects were calculated for each participant respectively. The behavioral index (BI) was used to characterize the behavioral facilitation in target detection by attentional modulation. Specifically, BI was calculated as BI = $(Contrast_{att} - Contrast_{neutral})/(Contrast_{att} + Contrast_{neutral})$, in which Contrast refers to the adjusted contrast for the target to be detected at an overall accuracy of 80%. The contrast threshold at the attended side was then compared to that for the neutral condition. The NI-parietal ($Alpha_{unatt} - Alpha_{neutral}$), which characterizes response difference between the unattended side for the cueing condition and that for the neutral condition (mean response within the significant time window, 0.14–0.2 s, Fig. 2D), was calculated on the alpha-band responses on the post-central parietal electrode (Fig. 3B right). The NI-occipital ($Alpha_{att} - Alpha_{neutral}$), which characterizes sensory response difference between the attended side for the cued condition and that for the neutral condition (mean response within the significant time window, 0.04–0.1 s, Fig. 3C), was calculated on the alpha-band responses on the occipital electrodes contralateral to the attended side (Fig. 3B left). Correlations between BI and the two neural indices (i.e., NI-parietal, NI-occipital) were calculated across participants respectively. The results of main experiment (N = 14) and control experiment (N = 6) have been used in the correlational analysis.

2.5.4. Granger causality analysis (GCA)

In order to study the strength and directionality of influences between the post-central parietal area and the contralateral occipital area, we employed Granger causality analysis (Granger, 1969), a statistical measure that quantifies the extent to which one time series can predict the other one. The principal idea behind GC is that if the addition of the history of signal A improves the prediction of signal B, as compared to the prediction of signal B based on its own history alone, then signal A is said to "Granger cause'' signal B. In the present study, we conducted GC in the frequency domain (Geweke, 1982). The result was a spectrum of causal influences between the parietal electrode and the occipital electrode as a function of frequency. The Pz was used as the post-central parietal electrode in which the power-changes are observable for both left and right stimuli. The PO8 (for left stimulus) and PO7 (for right stimulus) were used as contralateral occipital electrodes in which the power-changes are observable only for contralateral stimulus. Specifically, TRFs for cueing conditions (i.e., attend to left and attend to right) in the post-central parietal electrode and the contralateral occipital electrodes were put into the GCA analysis. Because stimuli were presented at both sides of the fixation, we computed Granger causality spectra in both the parietal-to-occipital (feedback, i.e., Pz-to-PO8 or Pz-to-PO7) and the occipital-to-parietal (feedforward, i.e., PO8-to-Pz or PO7-to-Pz) directions for the left and right stimulus, and for the attended and unattended conditions, in each subject, respectively. The Granger causality values were then averaged across conditions and stimuli within each participant, resulting in the parietal-to-occipital and occipital-to-parietal GC spectrum (as a function of frequency) for each subject. All participants (N = 20) from the main experiment (N = 14) and the control experiment (N = 6) were entered into the GCA analysis.

2.5.5. Statistical analysis

For the point-by-point statistics shown in Figs. 2D, 3C and 4A and B, and Fig. 5B, multiple comparisons were corrected using the false discovery rate (Benjamini and Hochberg, 1995). The activations in the parietal and occipital electrodes were examined using one-sample *t*-test against zero (Figs. 2D, 3C and 4A and 4B). Cluster-based permutation tests (Maris and Oostenveld, 2007) were used for examining topographic distribution difference (Fig. 3A), based on 500 permutations. Paired samples *t*-test comparing the alpha-band power for Att versus Neutral (Fig. 3A, left) and for Unatt versus Neutral (Fig. 3A, right) was performed for each sensor respectively. Sensors showing a significant effect ($p < 0.025$, 2-tailed) were then clustered based on spatial adjacency, with a minimum of 2 adjacent sensors to form a cluster. The clusters was further thresholded at an alpha level of 0.01 (two-tailed). We examined the latency differences in the alpha-band power course between the Att and Unatt conditions using a Jackknife approach (Miller et al., 1998). Specifically, we first calculated the peak latency for the Att - Neutral and Unatt - Neutral alpha-band power courses in the contralateral occipital electrodes, and this was done for each subject. Next, we iteratively removed one participant from the participant pool and computed the resulting latency difference. The Jackknife-based estimate of the standard error then allowed us to compare the observed latency difference against zero (i.e., the null hypothesis of no latency difference).

3. Results

We recorded 64-channel EEG signals from 20 participants fixating on a central spot while two discs were displayed simultaneously, in left and right visual fields respectively. As shown in Fig. 1A, at the beginning of the cueing trial, a central arrow cue indicated which side (left or right) the participants should attend to for target detection. The target only appeared in the cued disc (100% cue validity), and participants were informed of the cue validity (i.e., 100% cue validity here) in advance. In the neutral condition (Fig. 1B), the central bidirectional cue did not

contain target location information and the target would appear at either the left or right visual field with equal possibility. Importantly, using the same approach as we used before (Huang et al., 2018; Jia et al., 2017; Liu et al., 2017), the luminance of the two discs, in both cueing and neutral conditions, was independently modulated for 5 s, according to two 5 s random temporal sequence respectively (Fig. 1C). We next employed the TRF approach (Crosse et al., 2016) to calculate and separate neural impulse response for the two discs (Att TRF and Unatt TRF) from the same EEG recordings. The TRF method, which uses linear regression to quantify the linear part of the stimulus-response relationships, models the neural impulse response function (i.e., the evoked brain response to a unit change in luminance in a stimulus sequence as a function of time lag).

As illustrated in Fig. 1C, we first calculated the TRF responses for the attended, unattended, and neutral conditions in each channel and in each participant respectively (see representative participant data in Fig. 2A). We next performed a spectrotemporal analysis on the TRFs to examine their fine dynamic structures as a function of frequency (1–30 Hz) and time lag (0–0.8 s); this was done for each condition (Att, Unatt, Neutral), in each channel, and in each participant separately. Further analysis was then based on the spectrotemporal power pattern, in particular, the alpha-band power temporal profile of the TRF responses for each condition, based on previous findings supporting the critical role of alpha-band activity in visual attention (Haegens et al., 2012; Jia et al., 2017; Klimesch et al., 2007). Notably, the TRF spectrotemporal power difference between conditions might be not obvious in the temporal waveform since the grand average could cancel out the phase-inconsistent activities between subjects (Jia et al., 2017).

Fig. 2A illustrates the TRF responses of a representative participant on a representative sensor (Pz), and it is notable the TRF response became flat and noisy when the relationship between the stimulus sequence and the corresponding trial response was shuffled (achromatic lines), supporting that the calculated TRF waveform represented a genuine stimulus-specific tracking response (Fig. 2A, left; see the reconstruction in terms of the TRF response and conventional VEP in Supplementary Fig. 1). The TRF responses showed prominent alpha-band (8–12 Hz) activation (Fig. 2A, right; Fig. 2B, left), with a spatial distribution mainly in the post-parietal and occipital areas (Fig. 2B, right), also consistent with previous findings (Jia et al., 2017; VanRullen and Macdonald, 2012).

3.1. Post-central parietal alpha-band component

First, we compared the spectrotemporal power profiles between the Att and Unatt TRF responses (Att−Unatt), aiming to validate our previous findings (Jia et al., 2017). As shown in Fig. 2C, we observed a "decrease-followed-by-increase" alpha-band profile, consistent with our previous findings (Jia et al., 2017). Specifically, alpha-band activity for the attended stimulus decreased (Att < Unatt) within the first 200 ms temporal lag, followed by a subsequent rebound trend (Att > Unatt) within the next 200 ms temporal lag (Fig. 2C, left and middle). Topographical mapping of the alpha-band decrease revealed that the attentional effects occurred mainly over post-central parietal electrodes (Fig. 2C, right).

Meanwhile, direct comparisons between Att and Unatt conditions could not determine the exact underlying process. The decreased Att alpha-band response, the increased Unatt alpha-band activation, or both processes might cause the observed Att−Unatt decrease. We then compared the Att and Unatt TRFs with the Neutral TRFs respectively to dissociate the effects (see response for all the conditions in Supplementary Fig. 2). As shown in Fig. 2D, the Unatt−Neutral comparison showed a significant alpha-band increase in the first 200 ms temporal lag whereas the Att−Neutral comparison did not display any significant increase, indicating that the initial alpha-band decrease was mainly due to the enhancement on the unattended location. After the Unatt alpha-band (red line) enhancement within the first 200 ms temporal lag, the Att TRF (blue line) took turns to show a trend of alpha-band increase in the 200–400 ms temporal lag. Notably, also consistent with previous finding, the parietal alpha-band component displayed the same spatial distribution pattern for both left and right stimuli (see right panel of Fig. 3B for details) and did not show location-dependent lateralization effect.

Thus, in combination with previous findings, selective attention encompasses an alpha-band component in the post-central parietal area, which might coordinates resources by dynamically exerting inhibitions over locations (i.e., releasing attentional inhibition from the unattended item and switching to the attended item) and presumably represents a top-down modulation signal in high-level areas (Fig. 3B, right).

3.2. Contralateral occipital alpha-band component

As shown in Fig. 3A, comparing Att and Unatt with neutral condition respectively resulted in distinct spatial distribution maps. Specifically,

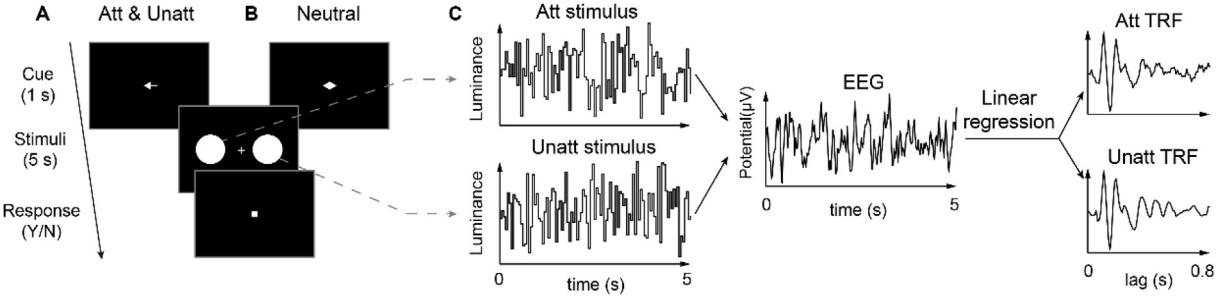

Fig. 1. Experimental paradigm and illustration of the temporal response function (TRF) approach. (A) Cued condition. An arrow cue appeared at the beginning of each trial to indicate which side the target would appear. Cue validity was 100%. Two discs were presented simultaneously in the left and right visual fields for 5 s, during which time participants were instructed to detect the appearance of a target square within the cued disc by pressing 1 of 2 response keys at the end of each trial. The target occurred at a random time so that participants had to maintain their attention on the cued disc. The contrast of the target square relative to the momentary disc luminance was adjusted trial by trial to maintain 80% detection performance overall. (B) Neutral condition. A diamond-shape neutral cue indicated that the target would appear at left or right sides with 50% probability. (C) The luminance of the 2 discs was independently and randomly modulated throughout the trial, according to 2 randomly generated 5 s random temporal sequences (e.g., left panel of Fig. 1C, top: attended luminance sequence, bottom: unattended luminance sequence). At the same time, electroencephalography (EEG) responses were recorded. The TRF approach was used to calculate the impulse brain responses for the attended (top, Att) and unattended (bottom, Unatt) locations. The obtained TRF characterizes the brain response to a unit increase in a luminance sequence, with the time axis representing the latency after each transient unit. Note that the Att TRF and Unatt TRF were derived from the same EEG responses based on the corresponding luminance sequence. The TRFs for the neutral condition were also calculated in the same way and averaged between the left and right stimuli.

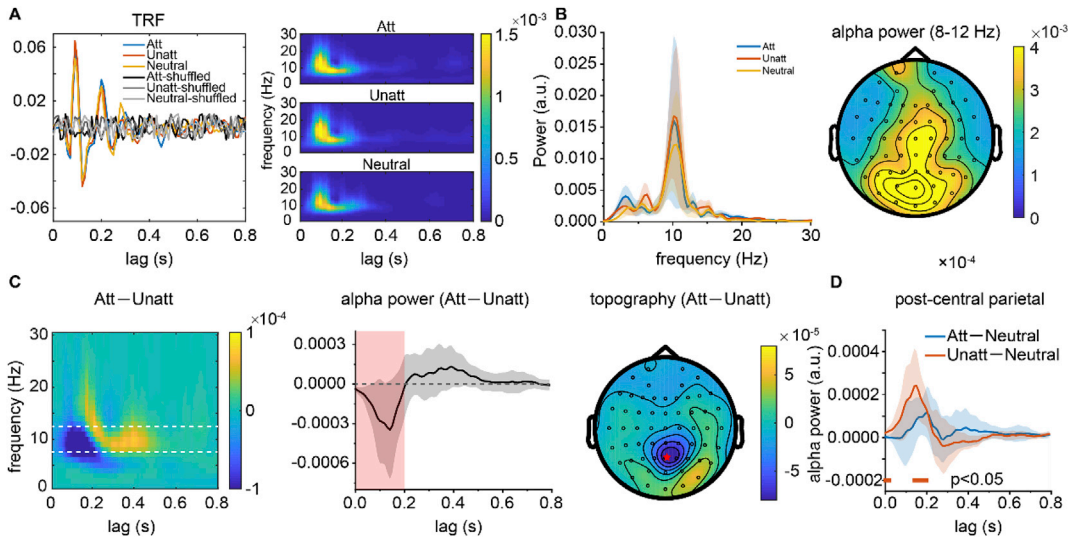

Fig. 2. Post-central parietal alpha-band component. (A) Left: TRF waveforms of a representative subject for attended, unattended, and neutral conditions as a function of latency (0–0.8 s). The achromatic lines represent TRF response when EEG signals and stimulus sequence were shuffled across trials. Right: corresponding time-frequency power profiles of the TRF responses. (B) Left: grand averaged (N = 14, shaded areas indicate 95% confidence interval) spectrum for TRF (0–0.8 s) for each condition. Right: topographic distribution of the alpha-power (8–12 Hz) of the TRF response averaged across three conditions. (C) Left: Grand averaged (N = 14) time-frequency representation for Att − Unatt on the post-central parietal electrode (Pz). Middle: Grand averaged (N = 14) alpha-band power time course (shaded area indicates 95% confidence interval) of Att − Unatt. Right: Grand averaged (N = 14) Att−Unatt distribution map of the alpha suppression (0–200 ms, red shades in the middle panel). (D) Grand averaged (N = 14) alpha-band power time courses (shaded areas indicate 95% confidence interval) of the post-central parietal electrode (Pz, red dot in the right panel of Figure 2C) for Att−Neutral (blue) and Unatt−Neutral (red). The horizontal lines at the bottom indicate time points at which the Att−Neutral (blue) and Unatt−Neutral (red) showed significant activation (paired *t*-test, $p < 0.05$, FDR corrected).

the Att−Neutral comparison showed significant activation in the bilateral occipital area (cluster-based permutation test, $p < 0.01$; Fig. 3A, left), whereas the Unatt−Neutral comparison mainly happened in the post-central parietal area (cluster-based permutation test, $p < 0.01$; Fig. 3A, right). We further divided targets based on where they were presented (left versus right), and then calculated the corresponding TRF response and the alpha-band power profiles separately. As shown in Fig. 3B, the left and right stimuli showed a spatial distribution map with contralateral lateralization patterns for Att−Neutral comparison (left panel), but not for Unatt−Neutral comparison (right panel). Further statistical analysis on the topographic difference between the left and right stimuli showed significant negative activations in the left hemisphere and positive activations in the right hemisphere for Att−Neutral (lower left). The contralateral occipital alpha-band activity is thus location-dependent and possibly represents sensory response in early visual areas (Fig. 3B, right).

We next assessed Att and Unatt TRFs in the contralateral occipital electrodes (i.e., the location-dependent channels, red star in Fig. 3B, upper left and middle left), by examining the corresponding alpha-band

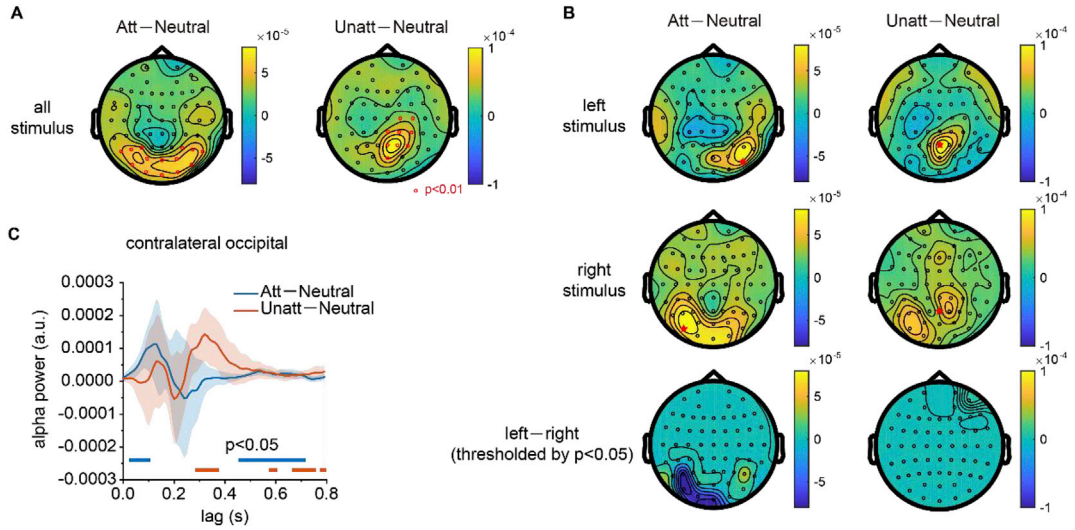

Fig. 3. Two alpha-band components: post-central parietal and contralateral occipital components. (A) Grand averaged (N = 14) topographic distribution map (0–200 ms in latency) for Att−Neutral (left) and Unatt−Neutral (right). The red dots indicate sensors showing significant clusters (cluster-based permutation test, $p < 0.01$). (B) Grand averaged (N = 14) topographic distribution map (0–200 ms in latency) for Att−Neutral (left) and Unatt−Neutral (right), when the stimulus is presented in the left (top) or right (middle) visual field. Bottom: Topographic distribution map (0–200 ms) for the left−right (threshold by $p < 0.05$) comparison of Att−Neutral (left) and Unatt−Neutral (right) conditions. (C) Grand averaged (N = 14) alpha-band power time courses of the occipital electrodes (PO8 for left stimulus and PO7 for right stimulus) for Att−Neutral (blue) and Unatt−Neutral (red) (shaded areas indicate 95% confidence interval). The horizontal lines at the bottom indicate time points at which the Att−Neutral (blue) and Unatt−Neutral (red) showed significant difference from zero (one-sample *t*-test, $p < 0.05$, FDR corrected).

temporal profiles for Att−Neutral and Unatt−Neutral comparisons (see alpha-band TRF responses for all the conditions in Supplementary Fig. 2). Interestingly, the occipital alpha-band activity in the TRF response displayed an "Att-followed-by-Unatt" temporal profile (Fig. 3C). Specifically, within the first 200 ms temporal lag, Att TRF showed an alpha-band enhancement (blue line), followed by the Unatt activation (red line) within the subsequent 200 ms temporal lag. The peak latencies for the alpha-band TRF response were different between the Att−Neutral and Unatt−Neutral comparisons (154.29 ± 28.71 ms; Jackknife procedure, $t_{(13)} = 5.37$, $p \leq 0.01$).

The new alpha-band component thus essentially differs from the previously observed parietal alpha-band component. First, it origins from sensory area and shows a location-specific contralateral response, whereas the parietal one is independent of stimulus location. Second, it showed enhancement for the attended than unattended locations within the first 200 ms temporal lag, whereas the parietal component displayed the reverse pattern (Att < Unatt within the first 200 ms temporal lag). The two alpha-band components might work together to coordinate attention over multiple locations.

3.3. Control experiment

In the previous design, cued and neutral conditions were presented in different blocks, and participants thus might have different attentional states in different blocks. We thus ran a control experiment (N = 6) using a random design by mixing the cued and netural conditions within the same block. As illustrated in Fig. 4, the mixed-design results were similar to our presvious results (Figs. 2 and 3). Specifically, the parietal alpha-band component showed enhanced Unatt−Neutral response during the first 200 ms temporal lag followed by a trend of increase in Att−Neutral response. The contralateral occipital alpha-band component again displayed delayed Unatt−Neutral response compared to Att−Neutral response (peak latency difference, Jackknife procedure, $t_{(5)} = 1.95$, $p = 0.054$, one-tail). Thus, the observed attentional effects were not due to the block design.

3.4. Behavioral relevance and parietal-occipital interactions

After establishing the two alpha-band components that occur in parietal and occipital areas respectively and are seemingly associated with distinct characteristics, we further examined their relevance to attentional behavior, as well as how the neural activities in parietal and occipital areas interact with each other.

First, we calculated the correlation coefficients between the behavior (behavioral index, BI) and the two alpha-band component activities (NI-parietal: neuronal index for parietal component; NI-occipital: neuronal index for the contralateral occipital component; see details in Methods) across participants, respectively. Specifically, the BI for each participant was calculated by comparing the adjusted target contrast between the attended and neutral conditions [$(Contrast_{att} - Contrast_{neutral})/(Contrast_{att} + Contrast_{neutral})$]. As shown in Fig. 5A, NI-parietal showed a strong negative correlation ($r = -0.47$, $p = 0.03$) with BI, such that stronger Unatt suppression (larger NI-parietal alpha-band activity) was accompanied by better target detection (lower target contrast, smaller BI), thus further supporting the inhibitory function of the parietal alpha-band component. In contrast, no correlation was found between NI-occipital and BI ($r = 0.03$, $p = 0.90$), and the two NIs did not show significant correlations either ($r = -0.12$, $p = 0.62$; Supplementary Fig. 3). Thus, only the parietal alpha-band component was associated with attentional behavior.

Next, we performed a Granger causality analysis between the post-central parietal and contralateral occipital areas to examine their relationships (i.e., parietal to occipital; occipital to parietal) as a function of frequency (0–40 Hz). The analysis was performed for the left and right stimuli and for each condition separately before combining them together. Fig. 5B plots the Granger causality spectrum results for parietal-to-occipital (blue; i.e., Pz-to-PO8 and Pz-to-PO7) and occipital-to-parietal (orange; i.e., PO8-to-Pz and PO7-to-Pz) directions. The parietal-to-occipital direction showed significantly larger causality values than the occipital-to-parietal direction within the alpha-band ($p < 0.05$, FDR corrected *t*-test), suggesting an essential role of alpha-band activities of the parietal area in modulating the sensory processing.

4. Discussion

In this study, we used EEG recordings in combination with a TRF approach to examine the spatiotemporal characteristics of neuronal impulse response in covert selective attention. In particular, we added a neutral condition to examine how the attended and unattended locations are processed respectively, and how the low-level sensory area engages in this process accordingly. First, consistent with previous findings, we demonstrated a parietal alpha-band component that is of essential behavioral relevance and mainly reflects the inhibition of the unattended stimulus. Second, we revealed a new contralateral alpha-band component in the occipital areas that has distinct characteristics. Finally, the parietal area exerted directional influences on the occipital activities through alpha-band modulation. Overall, our results support that selective spatial attention involves the coordination of two hierarchically organized alpha-band components that presumably serve distinct functions.

First, it is noteworthy that we employed a TRF approach to tag and dissociate the neural processing for the attended and unattended items. The TRF represents the impulse response, with the time axis indicating the latency after each frame of the stimulus sequence, thus characterizing

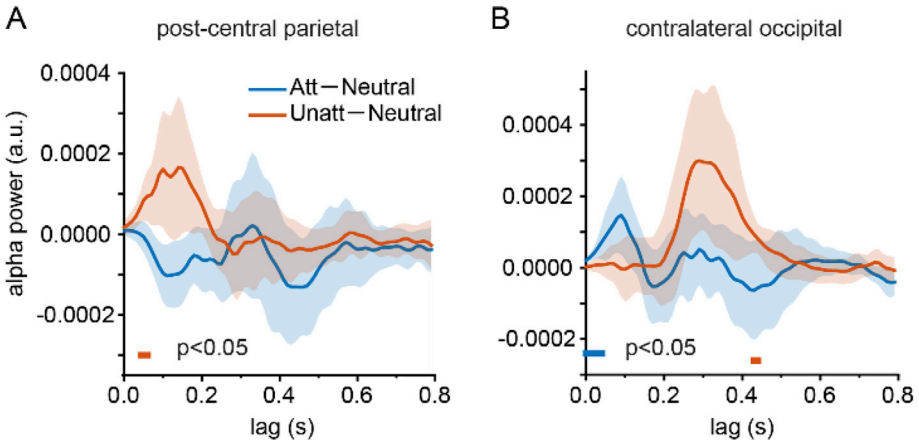

Fig. 4. Control experiment results (mixed design). (A) Grand averaged (N = 6) alpha-band power time courses for Att−Neutral (blue) and Unatt−Neutral (red) conditions on the post-central parietal electrode (i.e., Pz). (B) Grand averaged (N = 6) alpha-band power time courses for Att−Neutral (blue) and Unatt−Neutral (red) conditions on the contralateral occipital electrodes (PO8 for left stimulus and PO7 for right stimulus). The horizontal lines at the bottom indicate time points at which the Att−Neutral (blue) and Unatt−Neutral (red) showed significant activation (one-sample *t*-test, $p < 0.05$, FDR corrected). Shaded areas indicate 95% confidence interval.

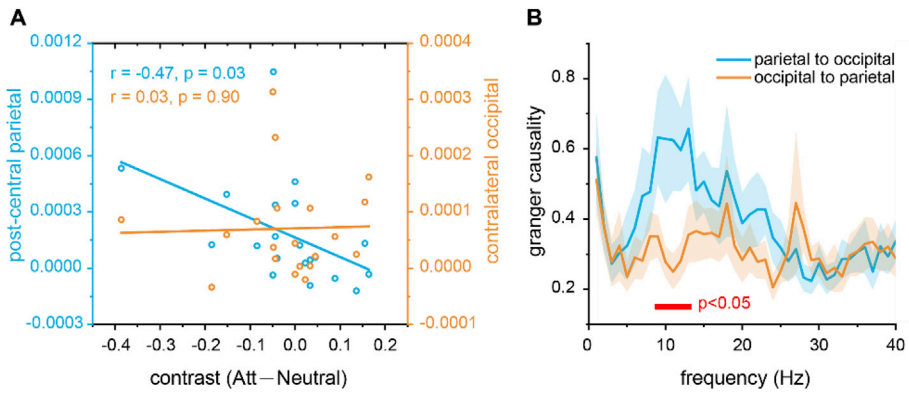

Fig. 5. Behavioral relevance and parietal-occipital interactions. (A) Correlation between behavioral performance (behavioral index, BI) and parietal (blue) and occipital (orange) alpha-band activities across 20 subjects (combining main experiment and control experiment). BI, parietal and occipital neural indices (NI) were calculated respectively for each subject. BI: $(Contrast_{att}-Contrast_{neutral})/(Contrast_{att}+Contrast_{neutral})$. NI-parietal: Unatt−Neutral response of the parietal electrode averaging over 0.14–0.2 s. NI-occipital: Att−Neutral response of the occipital electrodes averaging over 0.04–0.1 s. Only the NI-parietal showed significant negative correlation with BI. (B) Grand averaged (N = 20, main and control experiment) granger causality spectrum for parietal-to-occipital (blue, shaded area indicates 95% confidence interval; Pz-to-PO8 and Pz-to-PO7) and occipital-to-parietal (orange, shaded area indicates 95% confidence interval; PO8-to-Pz and PO7-to-Pz) direction. The horizontal red line at the bottom indicates the frequencies at which the parietal-to-occipital and the occipital-to-parietal direction showed significant difference (paired *t*-test, $p < 0.05$, FDR corrected).

a relative-time signal instead of absolute-time course (Crosse et al., 2016; Lalor et al., 2006). Therefore, the observed Att-Unatt temporal difference (i.e., 'sequential sampling' or 'sequential processing') in TRF responses primarily supports their temporal latency difference (defined relative to each luminance transient), and does not necessarily indicate an ongoing shifting between the two locations in absolute time within each trial, given the temporal summation of impulse responses across moments. Moreover, the TRF response and classical VEP have been found to be similar in many aspects (Lalor et al., 2006; Supplementary Fig. 1), and both of them may derive from stimulus-evoked response or reorganization of intrinsic brain oscillations (Makeig et al., 2002; VanRullen and Macdonald, 2012).

Consistent with previous findings (Buschman and Kastner, 2015; Fiebelkorn et al., 2018, 2013; Helfrich et al., 2018; Jia et al., 2017), our results support that even when attention is instructed to dwell on one spatial location over others throughout each trial, attention still intrinsically allocates resources to the out-of-focus locations. Specifically, attention sorts multiple locations over time according to their priority by first sampling the attended item followed by the unattended one. Recently, several psychophysical studies have revealed rhythmic structures in behavioral performance ('behavioral oscillation'), suggesting that multiple locations, features, and objects are processed alternatively over time (Fiebelkorn et al., 2013; Jia et al., 2017; Landau and Fries, 2012; Song et al., 2014). However, most of the studies have employed a divided attentional paradigm during which multiple locations are equally task-relevant, and therefore the oscillatory or sequential profiles might not generalize to the classical selective attention when only one of the locations is task-relevant. Our results, as well as our previous findings (Jia et al., 2017), by employing a selective attention task, thus constitute neural evidence supporting that the temporal organization or the sequential sampling plays a generally central function in attention. This view is also in line with a recent model proposing an oscillation-based temporal organization mechanism for processing task-irrelevant inputs (Buschman and Kastner, 2015; Jensen et al., 2014, 2012).

Interestingly, both the parietal and occipital alpha-band components showed sequential pattern or a trend of serial activation, supporting the idea that the sequential sampling may exist at hierarchical levels of visual attentional processing. This is consistent with previous studies revealing involvement of both early (Dugué et al., 2016; Kienitz et al., 2018) and high-level areas (Fiebelkorn et al., 2018; Helfrich et al., 2018; Jia et al., 2017; Landau et al., 2015) in attentional process. Moreover, single neuron in inferior colliculus has recently been shown to encode two simultaneous auditory stimuli by switching between their activity patterns (Caruso et al., 2018). Thus, the sequential sampling might arise from the interactions between low- and high-level areas.

A key observation in the current research concerns the inhibitory function of the post-central parietal alpha-band component, in line with previous results (Song et al., 2014; Jia et al., 2017). It is notable that although induced (i.e., non-phase-locked) alpha-band activities have been widely documented to reflect inhibitory states in attention (Haegens et al., 2012; Händel et al., 2011; Klimesch, 2012; Klimesch et al., 2007), the TRF response actually represents the phase-locking response for the luminance transient and thus could not be simply accounted for by previous inhibitory alpha-band findings. Moreover, this alpha-band component is independent of spatial locations and actually showed enhancement for the unattended versus attended stimulus, thus being also different from the lateralized phase-locked alpha-band activities as shown before (Herrmann, 2001; Keitel et al., 2019; Walter et al., 2012). The inhibitory phase-locked alpha-band component in the present study might reflect a periodic inhibition process, which resets the neural network so that attention would not be attached to only one item and the new incoming information could thus be processed (Buschman and Kastner, 2015; Kastner et al., 1999).

In addition to replicating the inhibitory central alpha-band component, we also demonstrated an alpha-band component in contralateral occipital electrode. We reason that this alpha-band component signifies sensory processing (i.e., attentional enhancement) in low-level areas. First, its location-dependent characteristics supports its origin from sensory areas (Herrmann, 2001; Keitel et al., 2019; VanRullen and Macdonald, 2012; Walter et al., 2012). Second, it would be more reasonable to interpret the "Att-followed-by-Unatt" alpha-band profile in terms of the view that the Att stimulus is given attentional priority and processed at a relatively earlier latency than the unattended one (noting the latency is defined in the relative timing of TRF response).

The two alpha-band component findings are also commensurate with a recent EEG study revealing independent alpha sources in occipital and parietal brain areas, with the two alpha-band activities modulated by attention in a different way (Sokoliuk et al., 2018). Moreover, by using an independent component analysis (ICA), previous study has demonstrated three components in EPRs – two lateral alpha-band components in the left and right occipital areas respectively and one central posterior alpha component (Makeig et al., 2002), and the parietal instead of occipital alpha-band activity influences the behavior (Gulbinaite et al., 2017). Our two-alpha results are thus consistent with these findings and constitute

new evidence for the dissociated functions of the parietal and occipital alpha-band components in attention.

The finding that post-central parietal area drives the contralateral occipital activity through alpha-band rhythm is also in line with recent studies (Jensen et al., 2015; Marshall et al., 2015; Michalareas et al., 2016; Popov et al., 2017). Feedforward and feedback signals have been proposed to be conveyed in the gamma-band and alpha-band respectively (Fries, 2015; Jensen et al., 2015; Jensen and Mazaheri, 2010; Michalareas et al., 2016; Popov et al., 2017; Spaak et al., 2012). In particular, the inhibitory alpha-band neuronal activity could mediate the top-down modulation by blocking the communication of local sensory activity to other neuronal groups (Zumer et al., 2014). Furthermore, high-level visual area such as frontal eye field (FEF) sends alpha-band feedback signals to the low-level areas to suppress the distractor (Cosman et al., 2018), prior to the stimulus-driven gamma-band activity in primary visual area (Popov et al., 2017).

5. Conclusion

Taken together, selective spatial attention involves the coordination of two hierarchically organized alpha-band components. The post-central parietal component might exert a top-down modulation on the low-level processing (i.e., contralateral occipital responses) by alternatively inhibiting locations one after another, leading to a temporally delayed (i.e., defined in relative timing of neural impulse response) response for the unattended stimulus in sensory area.

Conflicts of interest

The authors declare no conflicts of interest.

Acknowledgments

This work was supported by the National Natural Science Foundation of China (grant number 31571115 to H.L.) and Beijing Municipal Science & Technology Commission (Grants Z181100001518002). We thank Yingying Wang and Ying Fan for language editing during manuscript preparation.

Appendix A. Supplementary data

Supplementary data to this article can be found online at https://doi.org/10.1016/j.neuroimage.2019.05.079.

References

Benjamini, Y., Hochberg, Y., 1995. Controlling the false discovery rate: a practical and powerful approach to multiple testing. J. R. Stat. Soc. Ser. B 57, 289–300.
Buschman, T.J., Kastner, S., 2015. From behavior to neural dynamics: an integrated theory of attention. Neuron 88, 127–144. https://doi.org/10.1016/j.neuron.2015.09.017.
Carrasco, M., 2011. Visual attention: the past 25 years. Vis. Res. 51, 1484–1525. https://doi.org/10.1016/j.visres.2011.04.012.
Caruso, V.C., Mohl, J.T., Glynn, C., Lee, J., Willett, S.M., Zaman, A., Ebihara, A.F., Estrada, R., Freiwald, W.A., Tokdar, S.T., Groh, J.M., 2018. Single neurons may encode simultaneous stimuli by switching between activity patterns. Nat. Commun. 9, 2715. https://doi.org/10.1038/s41467-018-05121-8.
Cosman, J.D., Lowe, K.A., Woodman, G.F., Schall, J.D., 2018. Prefrontal control of visual distraction. Curr. Biol. 28, 414–420. https://doi.org/10.1016/j.cub.2017.12.023.
Crosse, M.J., Di Liberto, G.M., Bednar, A., Lalor, E.C., 2016. The multivariate temporal response function (mTRF) toolbox: a MATLAB toolbox for relating neural signals to continuous stimuli. Front. Hum. Neurosci. 10, 604. https://doi.org/10.3389/fnhum.2016.00604.
Davidson, M.J., Alais, D., van Boxtel, J.J., Tsuchiya, N., 2018. Attention periodically samples competing stimuli during binocular rivalry. eLife 7, e40868.
Desimone, R., 1998. Visual attention mediated by biased competition in extrastriate visual cortex. Phil. Trans. Biol. Sci. 353, 1245–1255. https://doi.org/10.1098/rstb.1998.0280.
Desimone, R., Duncan, J., 1995. Neural mechanisms of selective visual attention. Annu. Rev. Neurosci. 18, 193–222. https://doi.org/10.1146/annurev.ne.18.030195.001205.
Dugué, L., Roberts, M., Carrasco, M., 2016. Attention reorients periodically. Curr. Biol. 26, 1595–1601. https://doi.org/10.1016/j.cub.2016.04.046.
Fiebelkorn, I.C., Pinsk, M.A., Kastner, S., 2018. A dynamic interplay within the frontoparietal network underlies rhythmic spatial attention. Neuron 99, 842–853 e8. https://doi.org/10.1016/j.neuron.2018.07.038.
Fiebelkorn, I.C., Saalmann, Y.B., Kastner, S., 2013. Rhythmic sampling within and between objects despite sustained attention at a cued location. Curr. Biol. 23, 2553–2558. https://doi.org/10.1016/j.cub.2013.10.063.
Fries, P., 2015. Rhythms for cognition: communication through coherence. Neuron 88, 220–235. https://doi.org/10.1016/j.neuron.2015.09.034.
Geweke, J., 1982. Measurement of linear dependence and feedback between multiple time series. J. Am. Stat. Assoc. 77, 304–313. https://doi.org/10.1080/01621459.1982.10477803.
Granger, C.W.J., 1969. Investigating causal relations by econometric models and cross-spectral methods. Econometrica 37, 424–438. https://doi.org/10.2307/1912791.
Gulbinaite, R., İlhan, B., VanRullen, R., 2017. The triple-flash illusion reveals a driving role of alpha-band reverberations in visual perception. J. Neurosci. 37, 7219–7230. https://doi.org/10.1523/JNEUROSCI.3929-16.2017.
Haegens, S., Luther, L., Jensen, O., 2012. Somatosensory anticipatory alpha activity increases to suppress distracting input. J. Cogn. Neurosci. 24, 677–685. https://doi.org/10.1162/jocn_a_00164.
Händel, B.F., Haarmeier, T., Jensen, O., 2011. Alpha oscillations correlate with the successful inhibition of unattended stimuli. J. Cogn. Neurosci. 23, 2494–2502. https://doi.org/10.1162/jocn.2010.21557.
Helfrich, R.F., Fiebelkorn, I.C., Szczepanski, S.M., Lin, J.J., Parvizi, J., Knight, R.T., Kastner, S., 2018. Neural mechanisms of sustained attention are rhythmic. Neuron 99, 854–865 e5. https://doi.org/10.1016/j.neuron.2018.07.032.
Herrmann, C.S., 2001. Human EEG responses to 1-100 Hz flicker: resonance phenomena in visual cortex and their potential correlation to cognitive phenomena. Exp. Brain Res. 137, 346–353. https://doi.org/10.1007/s002210100682.
Ho, H.T., Leung, J., Burr, D.C., Alais, D., Morrone, M.C., 2017. Auditory sensitivity and decision criteria oscillate at different frequencies separately for the two ears. Curr. Biol. 27, 3643–3649 e3. https://doi.org/10.1016/j.cub.2017.10.017.
Huang, Q., Jia, J., Han, Q., Luo, H., 2018. Fast-backward replay of sequentially memorized items in humans. eLife 7, e35164. https://doi.org/10.1101/376202.
Huang, Y., Chen, L., Luo, H., 2015. Behavioral oscillation in priming: competing perceptual predictions conveyed in alternating theta-band rhythms. J. Neurosci. 35, 2830–2837. https://doi.org/10.1523/JNEUROSCI.4294-14.2015.
Jensen, O., Bonnefond, M., Marshall, T.R., Tiesinga, P., 2015. Oscillatory mechanisms of feedforward and feedback visual processing. Trends Neurosci. 38, 192–194. https://doi.org/10.1016/j.tins.2015.02.006.
Jensen, O., Bonnefond, M., VanRullen, R., 2012. An oscillatory mechanism for prioritizing salient unattended stimuli. Trends Cognit. Sci. 16, 200–206. https://doi.org/10.1016/j.tics.2012.03.002.
Jensen, O., Gips, B., Bergmann, T.O., Bonnefond, M., 2014. Temporal coding organized by coupled alpha and gamma oscillations prioritize visual processing. Trends Neurosci. 37, 357–369. https://doi.org/10.1016/j.tins.2014.04.001.
Jensen, O., Mazaheri, A., 2010. Shaping functional architecture by oscillatory alpha activity: gating by inhibition. Front. Hum. Neurosci. 4, 186. https://doi.org/10.3389/fnhum.2010.00186.
Jia, J., Liu, L., Fang, F., Luo, H., 2017. Sequential sampling of visual objects during sustained attention. PLoS Biol. 15, e2001903. https://doi.org/10.1371/journal.pbio.2001903.
Kastner, S., Pinsk, M.A., De Weerd, P., Desimone, R., Ungerleider, L.G., 1999. Increased activity in human visual cortex during directed attention in the absence of visual stimulation. Neuron 22, 751–761.
Keitel, C., Keitel, A., Benwell, C.S.Y., Daube, C., Thut, G., Gross, J., 2019. Stimulus-driven brain rhythms within the alpha band: the attentional-modulation conundrum. J. Neurosci. 39, 3119–3129. https://doi.org/10.1523/JNEUROSCI.1633-18.2019.
Kienitz, R., Schmiedt, J.T., Shapcott, K.A., Kouroupaki, K., Saunders, R.C., Schmid, M.C., 2018. Theta rhythmic neuronal activity and reaction times arising from cortical receptive field interactions during distributed attention. Curr. Biol. 28, 2377–2387. https://doi.org/10.1016/j.cub.2018.05.086.
Klimesch, W., 2012. Alpha-band oscillations, attention, and controlled access to stored information. Trends Cognit. Sci. 16, 606–617. https://doi.org/10.1016/j.tics.2012.10.007.
Klimesch, W., Sauseng, P., Hanslmayr, S., 2007. EEG alpha oscillations: the inhibition–timing hypothesis. Brain Res. Rev. 53, 63–88. https://doi.org/10.1016/j.brainresrev.2006.06.003.
Lalor, E.C., Pearlmutter, B.A., Reilly, R.B., McDarby, G., Foxe, J.J., 2006. The VESPA: a method for the rapid estimation of a visual evoked potential. Neuroimage 32, 1549–1561. https://doi.org/10.1016/j.neuroimage.2006.05.054.
Landau, A.N., Fries, P., 2012. Attention samples stimuli rhythmically. Curr. Biol. 22, 1000–1004. https://doi.org/10.1016/j.cub.2012.03.054.
Landau, A.N., Schreyer, H.M., van Pelt, S., Fries, P., 2015. Distributed attention is implemented through theta-rhythmic gamma modulation. Curr. Biol. 25, 2332–2337. https://doi.org/10.1016/j.cub.2015.07.048.
Large, E.W., Jones, M.R., 1999. The dynamics of attending: how people track time-varying events. Psychol. Rev. 106, 119–159. https://doi.org/10.1037/0033-295X.106.1.119.
Liu, L., Wang, F., Zhou, K., Ding, N., Luo, H., 2017. Perceptual integration rapidly activates dorsal visual pathway to guide local processing in early visual areas. PLoS Biol. 15, e2003646. https://doi.org/10.1371/journal.pbio.2003646.
Makeig, S., Westerfield, M., Jung, T.-P., Enghoff, S., Townsend, J., Courchesne, E., Sejnowski, T.J., 2002. Dynamic brain sources of visual evoked responses. Science 295, 690–694. https://doi.org/10.1126/science.1066168.

Maris, E., Oostenveld, R., 2007. Nonparametric statistical testing of EEG- and MEG-data. J. Neurosci. Methods 164, 177–190. https://doi.org/10.1016/j.jneumeth.2007.03.024.

Marshall, T.R., O'Shea, J., Jensen, O., Bergmann, T.O., 2015. Frontal eye fields control attentional modulation of alpha and gamma oscillations in contralateral occipitoparietal cortex. J. Neurosci.: the official journal of the Society for Neuroscience 35, 1638–1647. https://doi.org/10.1523/JNEUROSCI.3116-14.2015.

Michalareas, G., Vezoli, J., van Pelt, S., Schoffelen, J.-M., Kennedy, H., Fries, P., 2016. Alpha-beta and gamma rhythms subserve feedback and feedforward influences among human visual cortical areas. Neuron 89, 384–397. https://doi.org/10.1016/j.neuron.2015.12.018.

Miller, J., Patterson, T., Ulrich, R., 1998. Jackknife-based method for measuring LRP onset latency differences. Psychophysiology 35, 99–115. https://doi.org/10.1111/1469-8986.3510099.

Oostenveld, R., Fries, P., Maris, E., Schoffelen, J.-M., 2011. FieldTrip: open source software for advanced analysis of MEG, EEG, and invasive electrophysiological data. Comput. Intell. Neurosci. 1–9, 2011. https://doi.org/10.1155/2011/156869.

Popov, T., Kastner, S., Jensen, O., 2017. FEF-controlled alpha delay activity precedes stimulus-induced gamma-band Activity in visual cortex. J. Neurosci. 37, 4117–4127. https://doi.org/10.1523/JNEUROSCI.3015-16.2017.

Schroeder, C.E., Lakatos, P., 2009. Low-frequency neuronal oscillations as instruments of sensory selection. Trends Neurosci. 32, 9–18. https://doi.org/10.1016/j.tins.2008.09.012.

Sokoliuk, R., Mayhew, S.D., Aquino, K., Wilson, R., Brookes, M.J., Francis, S.T., Hanslmayr, S., Mullinger, K.J., 2018. Two spatially distinct posterior alpha sources fulfill different functional roles in attention. bioRxiv. https://doi.org/10.1101/384065.

Song, K., Meng, M., Chen, L., Zhou, K., Luo, H., 2014. Behavioral oscillations in attention: rhythmic α pulses mediated through θ band. J. Neurosci. 34, 4837–4844. https://doi.org/10.1523/JNEUROSCI.4856-13.2014.

Spaak, E., Bonnefond, M., Maier, A., Leopold, D.A., Jensen, O., 2012. Layer-specific entrainment of gamma-band neural activity by the alpha rhythm in monkey visual cortex. Curr. Biol. 22, 2313–2318. https://doi.org/10.1016/j.cub.2012.10.020.

Tsotsos, J.K., 1990. Analyzing vision at the complexity level. Behav. Brain Sci. 13, 423–445. https://doi.org/10.1017/S0140525X00079577.

VanRullen, R., Macdonald, J.S.P., 2012. Perceptual echoes at 10 Hz in the human brain. Curr. Biol. 22, 995–999. https://doi.org/10.1016/j.cub.2012.03.050.

Walter, S., Quigley, C., Andersen, S.K., Mueller, M.M., 2012. Effects of overt and covert attention on the steady-state visual evoked potential. Neurosci. Lett. 519, 37–41. https://doi.org/10.1016/j.neulet.2012.05.011.

Wang, Y., Luo, H., 2017. Behavioral oscillation in face priming: prediction about face identity is updated at a theta-band rhythm. Progress in Brain Research. Elsevier, pp. 211–224. https://doi.org/10.1016/bs.pbr.2017.06.008.

Zumer, J.M., Scheeringa, R., Schoffelen, J.-M., Norris, D.G., Jensen, O., 2014. Occipital alpha activity during stimulus processing gates the information flow to object-selective cortex. PLoS Biol. 12, e1001965. https://doi.org/10.1371/journal.pbio.1001965.